Supporting Information

FeCo-Anchored Reduced Graphene Oxide Framework-Based Soft Composites Containing Carbon Nanotubes as Highly Efficient Microwave Absorbers with Excellent Heat Dissipation Ability

Injamamul Arief,[†] Sourav Biswas,[‡] Suryasarathi Bose*[,†]

[†]*Department of Materials Engineering, Indian Institute of Science, Bangalore, India 560012.*

[‡]*Department of Chemistry, National Institute of Technology Durgapur 713209, West Bengal, India.*

* sbose@materials.iisc.ernet.in (S.B.).

Table of contents

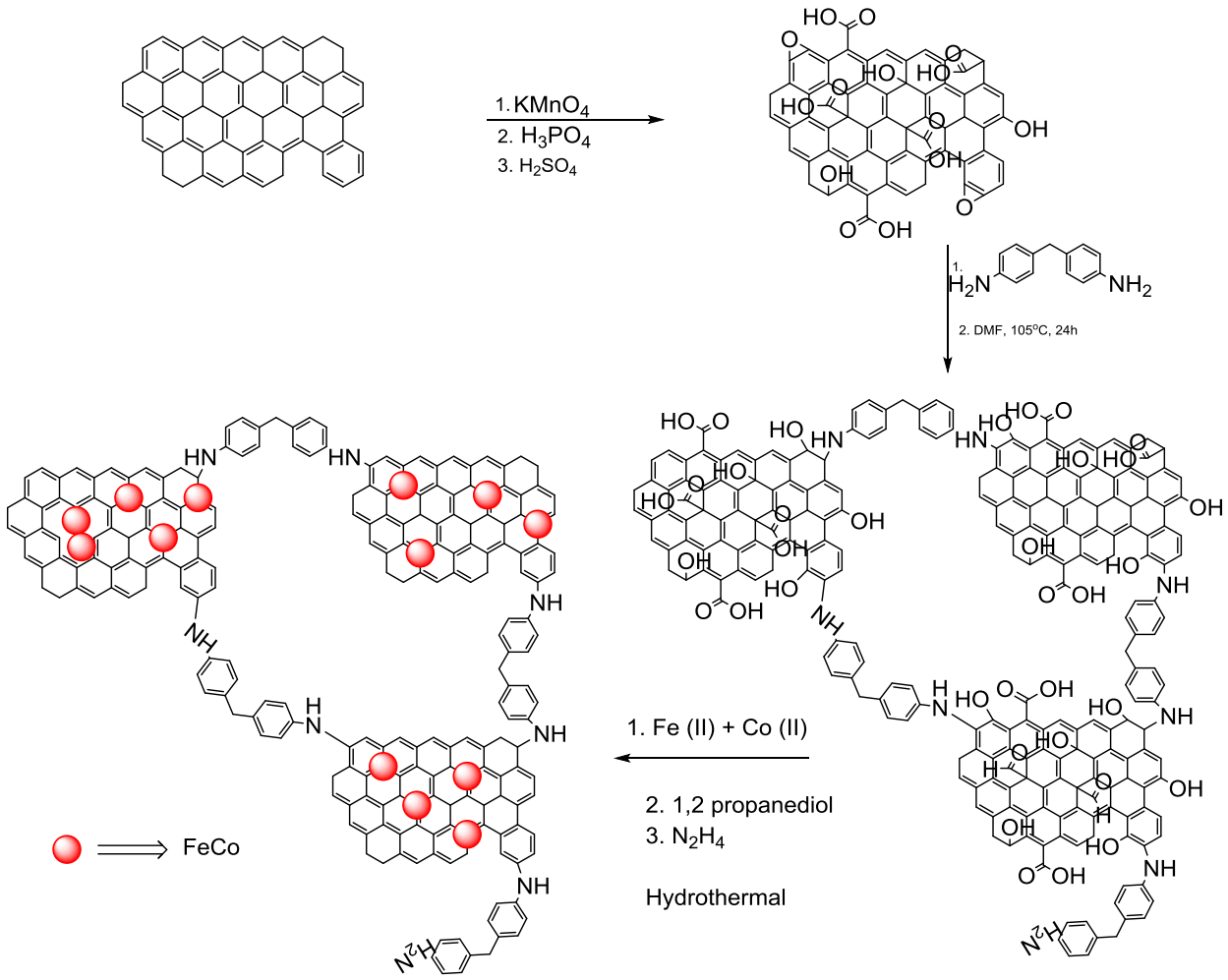

Figure S1: The possible mechanism and pathways for the reaction to form GO-MDA and rGO/MDA/FeCo structures.

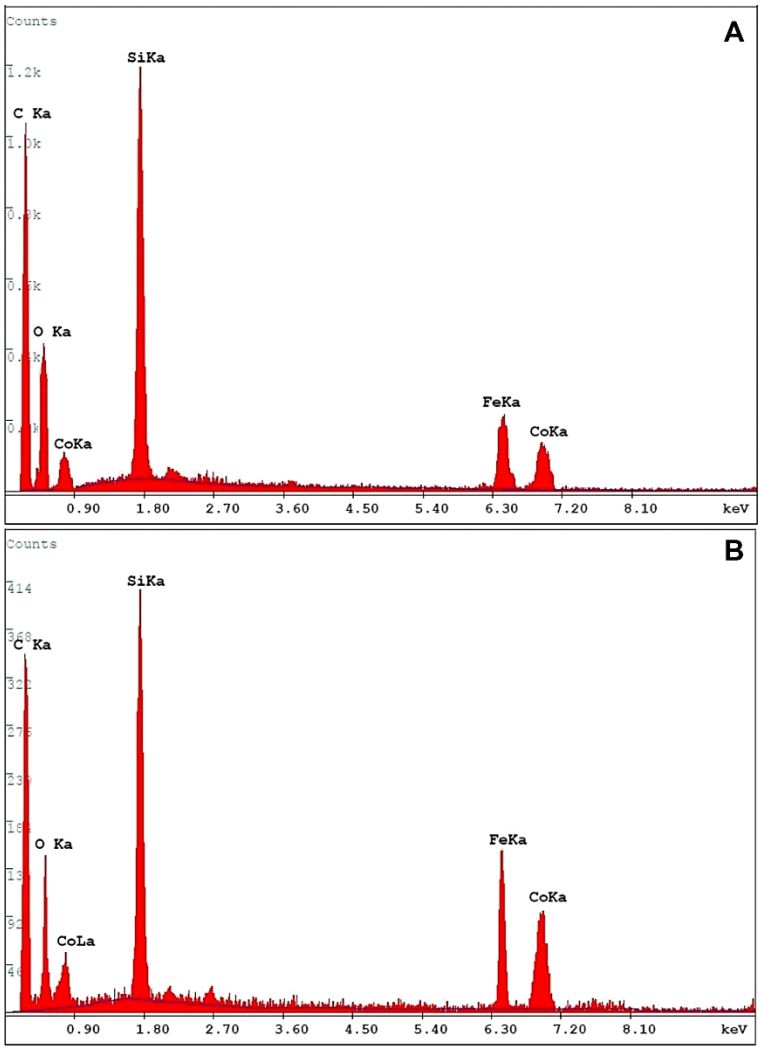

Figure S2: The EDAX spectra of the cross-linked rGO/FeCo samples; (A) rGO-MDA-FeCo1 and (B) rGO-MDA-FeCo2, illustrate that the contribution from both the elements of Fe and Co was equimolar in the cross-linked composites, thus corroborating with that of the initial molar concentrations.

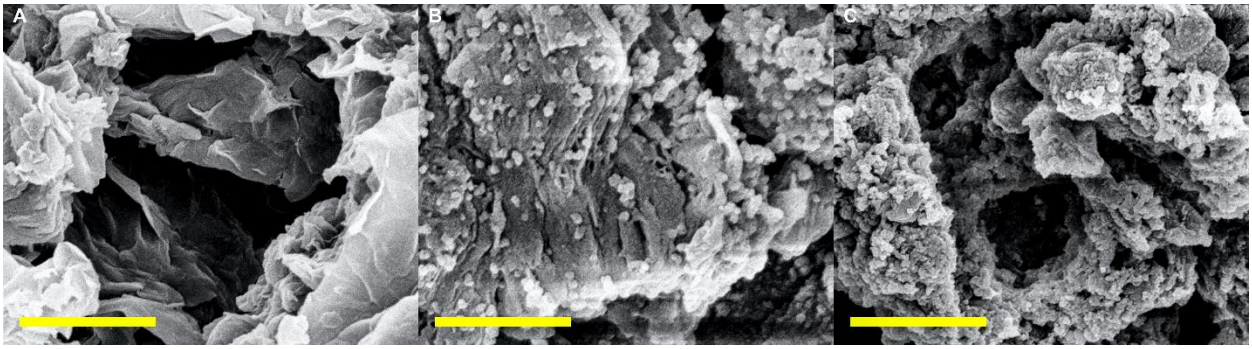

Figure S3: Higher magnification FESEM images of highly porous GO-MDA networks structures; (A) porous nanostructures of GO-MDA, (B) rGO-MDA-FeCo1 and (C) rGO-MDA-FeCo2. From the images, it is observed that the rGO/FeCo largely retain their porous 3D morphology. The scale bar measures 200 nm.

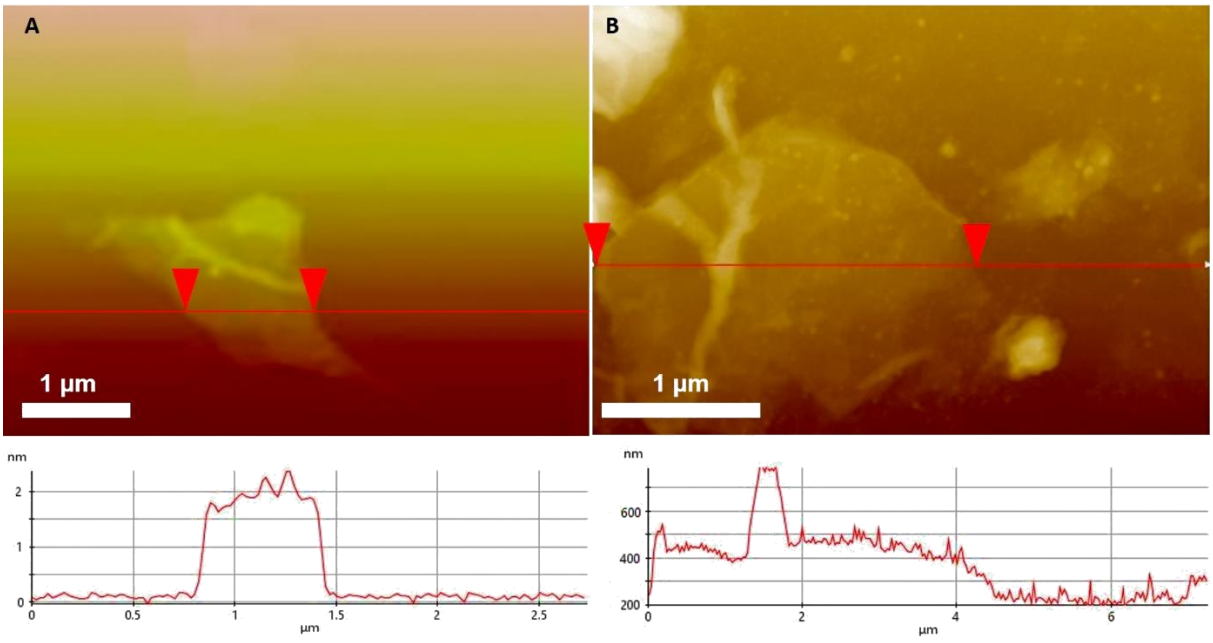

Figure S4: Topographical Tapping Mode AFM image of the as-synthesized GO (A) and rGO-MDA-FeCo1 (B). The thickness of GO on the Si-substrate calculated from the line profile below and found to be ~ 2 nm, which indicates a possible double-layer GO conformation. The thickness of rGO/FeCo structure is increased manifolds, indicating cross-linked network formation which sustained during the reduction of GO to rGO.

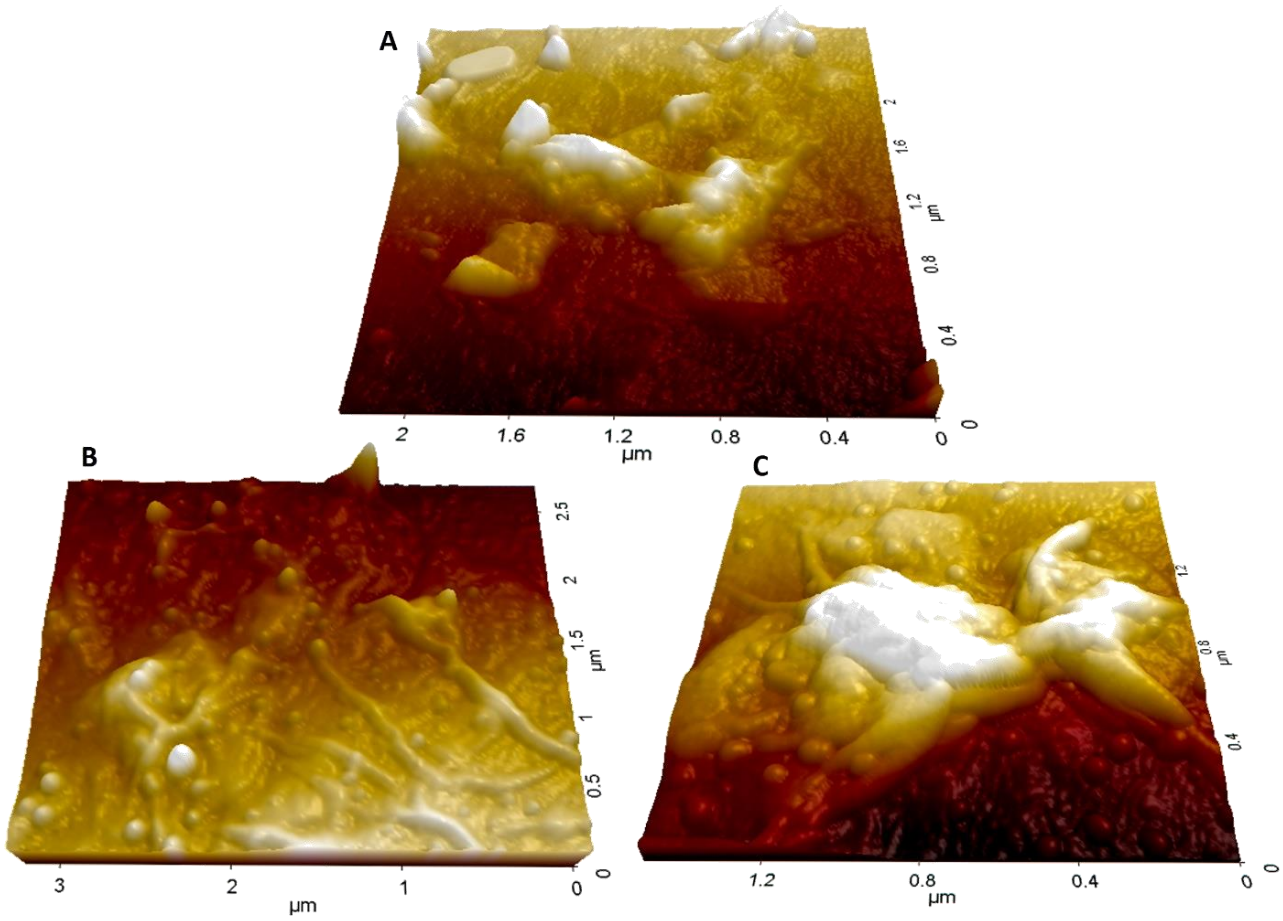

Figure S5: The 3D topographical features of GO-MDA (A), rGO-MDA-FeCo1 (B) and rGO-MDA-FeCo2 (C) are shown below. The typical roughness with highly porous wrinkled morphology is associated with the 3D cross-linked features of the N-conjugated GO frameworks, thus echoing SEM and TEM findings.

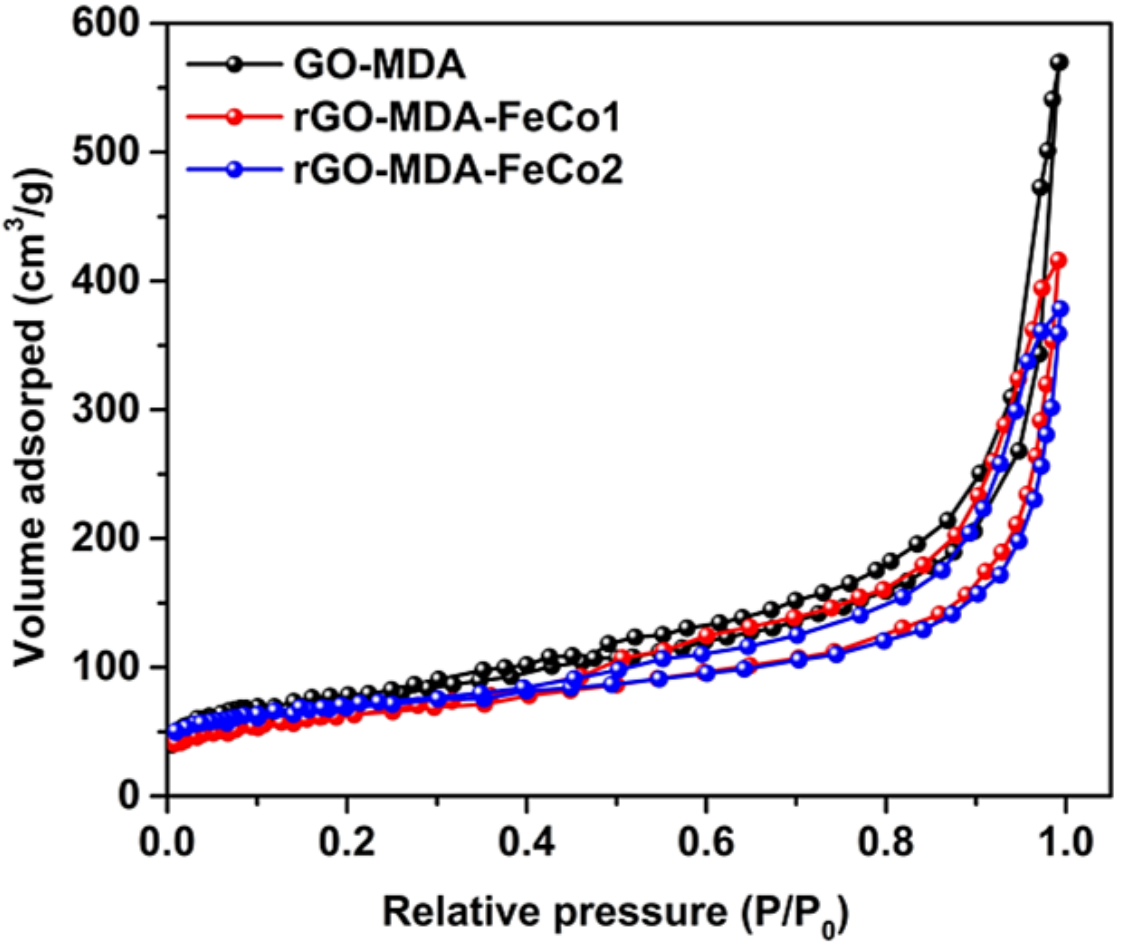

Figure S6: The porosity and specific surface areas of the cross-linked GO-MDA and FeCo-rGO-derivatives were analyzed by nitrogen adsorption-desorption isotherms measured at 77K.

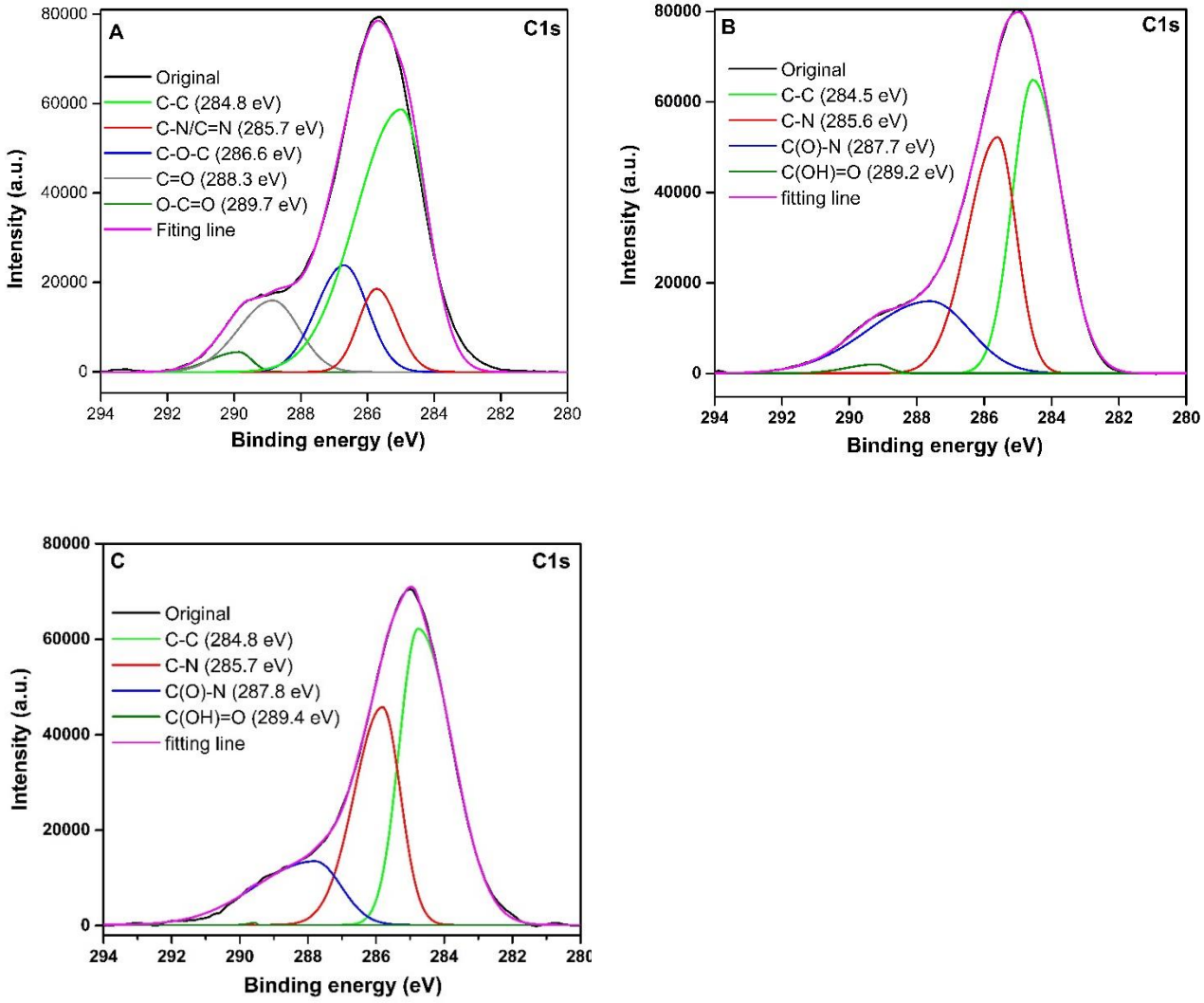

Figure S7: XPS elemental analyses of GO-MDA network (A), rGO-MDA-FeCo1 (B) and rGO-MDA-FeCo2 (C) structures in the C 1s region. The GO-MDA exhibits five characteristic peaks following Gaussian fitting of the C1s- namely C-C, C=N, C-O-C, C=O and O-C=O correspond to binding energies of 284.8 eV, 285.7 eV, 286.6 eV, 288.3 eV and 289.7 eV, respectively. Absence of epoxy and carbonyl peaks indicates crosslinking and reduction phenomena in the rGO/FeCo materials.

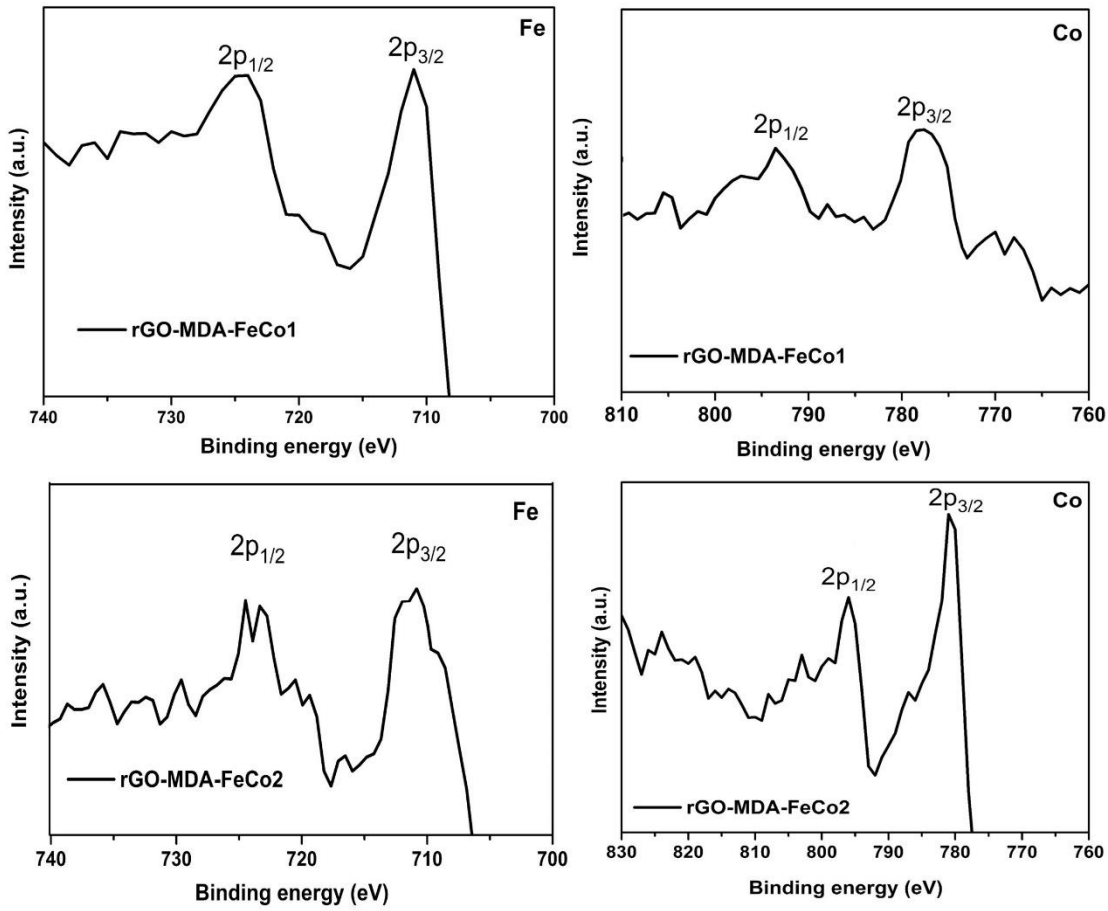

Figure S8: XPS spectra of Fe 2p and Co 2p regions in the rGO-MDA-FeCo1 and rGO-MDA-FeCo2, respectively. The peaks at 778.5 eV and 793.2 eV (Figure S8) in rGO-MDA-FeCo1 are assigned to be of Co $2p_{3/2}$ and Co $2p_{1/2}$, respectively. Similarly, peaks positioned at 793.1 eV and 779 eV in rGO-MDA-FeCo2 are associated to the spin-orbit splitting of Co $2p_{1/2}$ and Co $2p_{3/2}$, respectively.

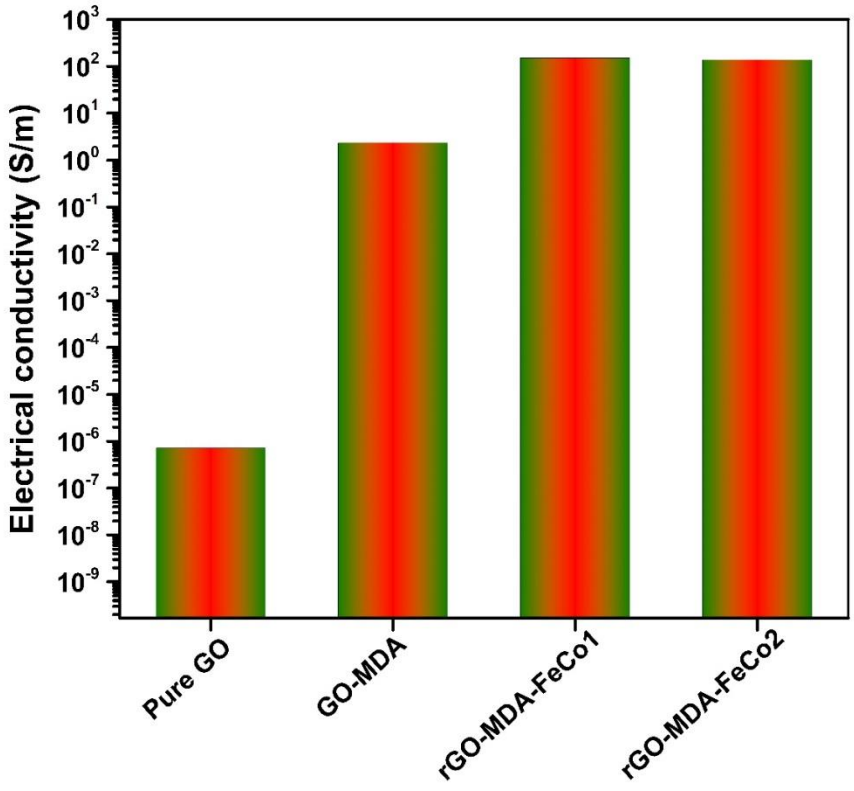

Figure S9: Electrical conductivity values of GO and its cross-linked network structures.

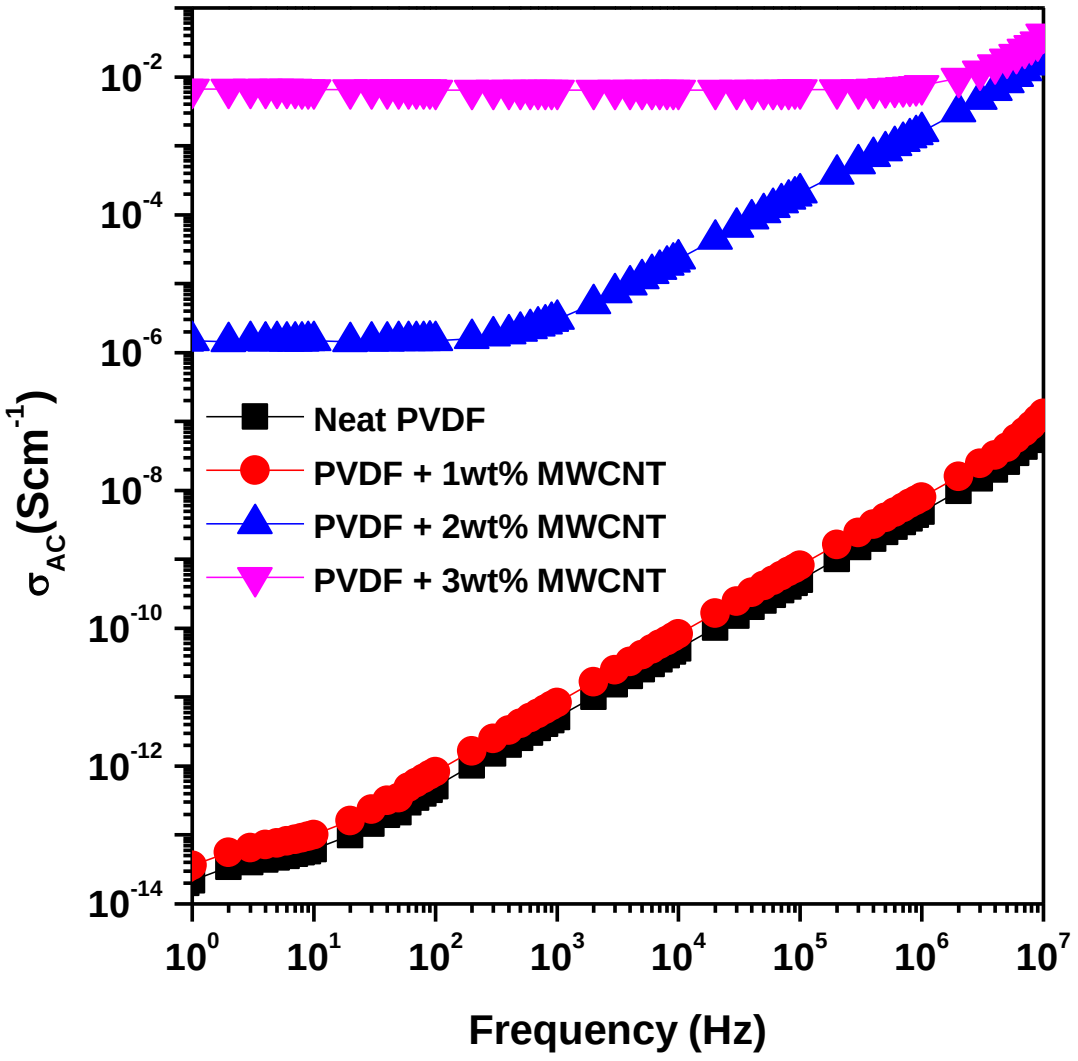

Figure S10: AC electrical conductivity plot with different MWCNTs concentration

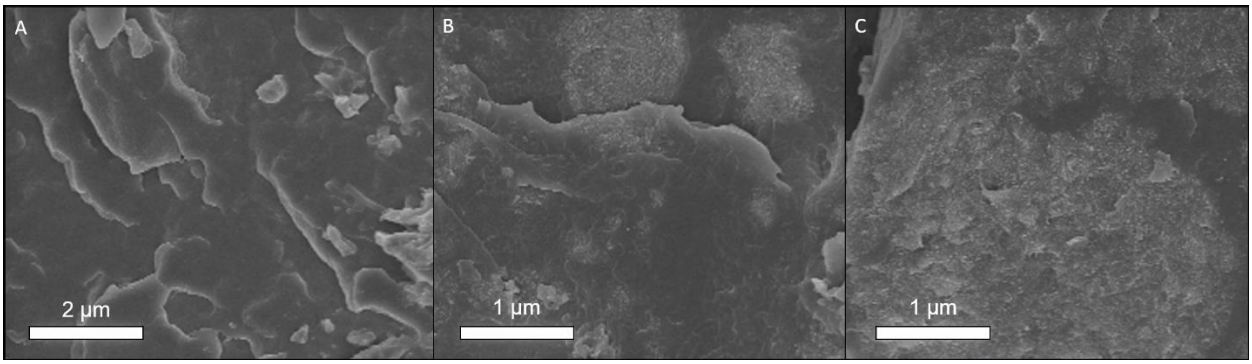

Figure S11: SEM images show the morphology of PVDF with 3 wt% MWCNT+10 wt% GO-MDA (A), PVDF with 3 wt% MWCNT+10 wt% rGO-MDA-FeCo1 (B) and PVDF with 3 wt% MWCNT+10 wt% rGO-MDA-FeCo2 (C). The quality of dispersion is quite decent for the various GO-based network fillers designed.

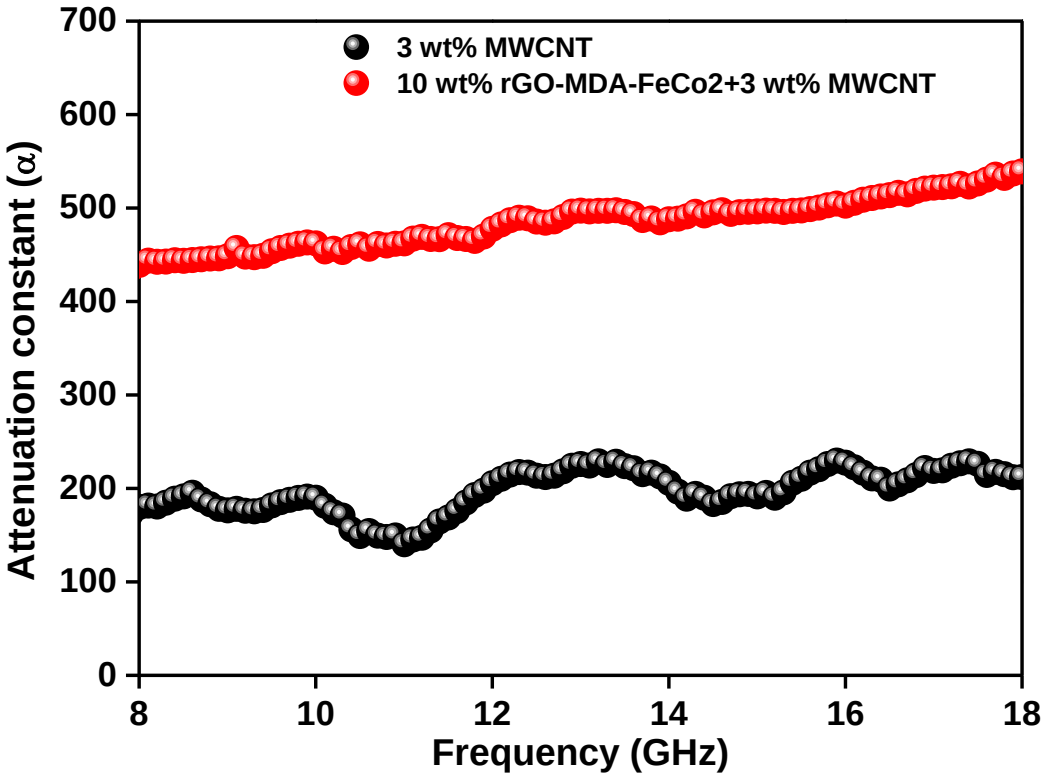

Figure S12: Attenuation constant of various composite structures in terms of frequency.

The attenuation constant (α) is quantitatively associated to the ability of EM absorption and can be evaluated by the corresponding permittivity and permeability parameters. Higher magnetic and dielectric losses are indispensable to improved EM attenuation. The formation of cross-linked structure of GO-MDA enhances the permittivity value of the composite structure due to its higher dielectric loss parameters as well as saturation magnetization and magnetic inclusion by FeCo decoration directly enhances magnetic permeability, which has massive influence in enhancing the attenuation constant value.

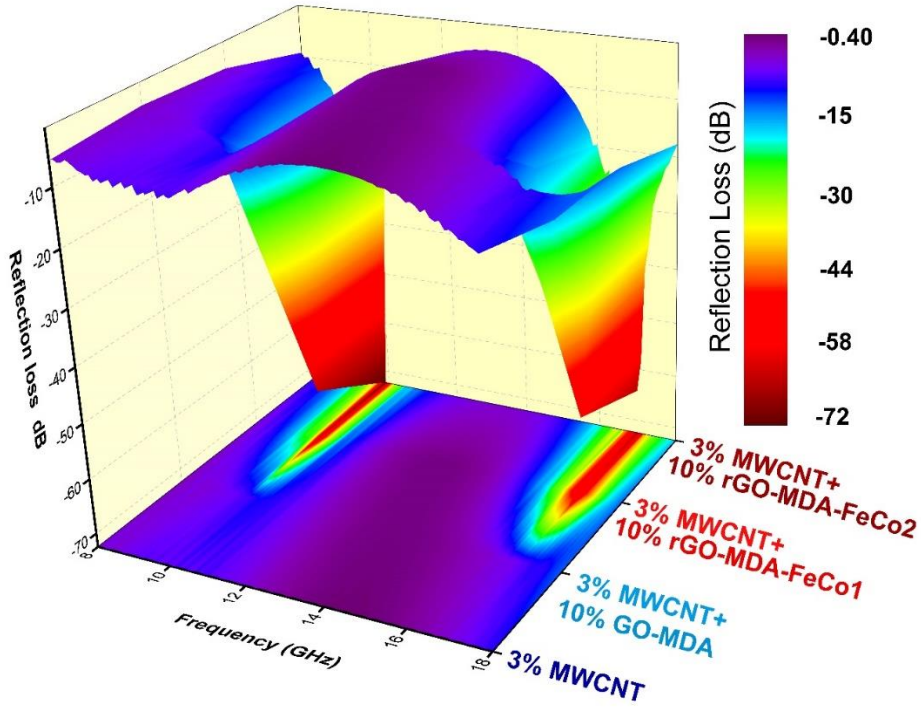

Figure S13: 3D representation of Reflection loss (R_L) of various nanocomposites in terms of frequency (sample thickness 5 mm). R_L of various nanocomposites from well-established Line Theory by Nicolson and Ross. In general R_L is dependent on the permittivity and permeability values (μ_r, ε_r) as follows;

$$R_L = 20 \log (|Z_{in} - 1|/| Z_{in} + 1|)$$

$$Z_{in} = (\mu_r/\varepsilon_r)^{1/2} \tanh\{j\frac{2\pi}{c}(\mu_r/\varepsilon_r)^{1/2} ft\}$$

where, sample thickness is represented by *t* and velocity of light is represented by *c*. In general reflection loss is generated due to the polarization, Ohmic losses and by multiple

reflection. A significant change is observed here after incorporation of FeCo nanoparticles into the rGO network along with MWCNTs due to enhanced dielectric and magnetization behavior.

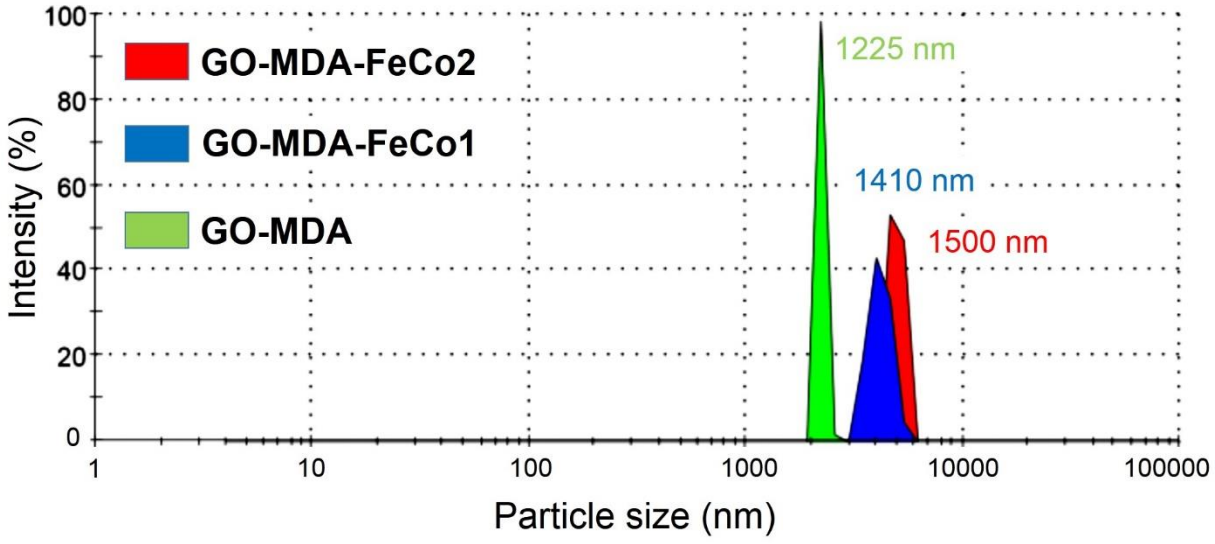

Figure S14: Average particle size distribution histogram obtained from DLS measurements for GO-MDA and rGO/FeCo-based aqueous dispersions. Due to crosslinking followed by *in situ* reduction of GO and Fe & Co-salts to form FeCo, the effective lateral size increases.

Table S1. Specific surface area and pore volume of GO-MDA and the FeCo-rGO-derivatives. For each sample, two measurements were performed and the values were averaged.

Sample name	Surface area ($m^2 g^{-1}$)	Pore volume ($cm^3 g^{-1}$)
GO-MDA	267.45	0.85
rGO-MDA-FeCo1	218.30	0.72
rGO-MDA-FeCo2	201.84	0.67

Table S2: Elemental analyses of GO, cross-linked GO-MDA and rGO/FeCo based systems.

Sample name	C (%)	O (%)	N (%)
GO	64.3	31.2	Nil (noise)
GO-MDA	71.6	20.5	6.2
rGO-MDA-FeCo1	77.6	11.8	7.5
rGO-MDA-FeCo2	78.8	10.6	7.8

Table S3: Total shielding effectiveness of various composite blends at 18 GHz frequency

Compositions	Total Shielding Effectiveness (dB)
PVDF	0
PVDF with 2 wt% MWCNT	-10
PVDF with 3 wt% MWCNT	-18
PVDF with 3 wt% MWCNT and 10wt% GO	-20
PVDF with 10wt% GO	-2
PVDF with 3 wt% MWCNT and 10 wt% cross-linked GO-MDA	-22
PVDF with 10 wt% cross-linked GO-MDA	-3
PVDF with 3 wt% MWCNT and 10 wt% cross-linked rGO-MDA-FeCo1	-35
PVDF with 3 wt% MWCNT and 10 wt% cross-linked rGO-MDA-FeCo2	-41.2
PVDF with 10 wt% cross-linked rGO-MDA-FeCo2	-12

Table S4: Comparison of EMI shielding properties of various composites containing 3D graphene/ rGO-magnetic particles

Matrix	Nanoparticles/fillers	Frequency (GHz)	Thickness (mm)	SE_{Total} (dB)	RL (dB)	Ref.
PANI	Graphene/Fe_3O_4	12-18	2.5	-32.3	-	[1]
Paraffin	Graphene 3D nanocapsules/Fe_3O_4 (50 wt%)	2-18 (8.76)	3.5	-	-32	[2]
-	rGO-Ni (Ni@ 63.2 wt%) composites	2-18 (7.5)	3	-	-23.3	[3]
PC-SAN	RGO-Co/MWCNT (10 wt% +3 wt%)	12-18 (18)	5	-34	-	[4]
PVDF	RGO-Co_3O_4 (10 wt%)	2-18 (11.6)	4	-	-25	[5]
PANI	RGO-γFe_2O_3 (75 wt%)	12-18 (11.3)	2.5	-51	-	[6]
-	3D Graphene/(Pt, Ag) composites	8.2-12.4	0.8	-28 (av.)	-	[7]
Epoxy	3D Graphene Aerogel (1 wt%)	10-20	3	-30	-	[8]
PVDF	RGO-$MnFe_2O_4$ (5 wt%)	2-18 (9.2)	3	-29	-	[9]
PVDF	3D cross-linked RGO-FeCo (10 wt%) + 3 wt% MWCNT	12-18	5	-41	-	This work

References:

1. Singh, K.; Ohlan, A.; Pham, V. H.; Balasubramaniyan, R.; Varshney, S.; Jang, J.; Hur, S. H.; Choi, W. M.; Kumar, M.; Dhawan, S., Nanostructured Graphene/Fe 3 O 4 Incorporated Polyaniline as a High Performance Shield Against Electromagnetic Pollution. *Nanoscale* **2013,** *5* (6), 2411-2420.
2. Jian, X.; Wu, B.; Wei, Y.; Dou, S. X.; Wang, X.; He, W.; Mahmood, N., Facile Synthesis of Fe3O4/GCs Composites and Their Enhanced Microwave Absorption Properties. *ACS Appl. Mater. Interfaces* **2016,** *8* (9), 6101-6109.
3. Wang, X.; Yu, M.; Zhang, W.; Zhang, B.; Dong, L., Synthesis and Microwave Absorption Properties of Graphene/Nickel Composite Materials. *Appl. Phys. A* **2015,** *118* (3), 1053-1058.
4. Pawar, S. P.; Bose, S., Extraordinary Synergy in Attenuating Microwave Radiation with Cobalt-Decorated Graphene Oxide and Carbon Nanotubes in Polycarbonate/Poly (styrene-co-acrylonitrile) Blends. *ChemNanoMat* **2015,** *1* (8), 603-614.
5. Wang, G. S.; Wu, Y.; Wei, Y. Z.; Zhang, X. J.; Li, Y.; Li, L. D.; Wen, B.; Yin, P. G.; Guo, L.; Cao, M. S., Fabrication of Reduced Graphene Oxide (RGO)/Co3O4 Nanohybrid Particles and a RGO/Co3O4/Poly (vinylidene fluoride) Composite with Enhanced Wave-Absorption Properties. *ChemPlusChem* **2014,** *79* (3), 375-381.
6. Singh, A. P.; Mishra, M.; Sambyal, P.; Gupta, B. K.; Singh, B. P.; Chandra, A.; Dhawan, S., Encapsulation of γ-Fe 2 O 3 Decorated Reduced Graphene Oxide in Polyaniline Core–Shell Tubes as an Exceptional Tracker for Electromagnetic Environmental Pollution. *J. Mater. Chem. A* **2014,** *2* (10), 3581-3593.

7. Sahoo, P.; Aepuru, R.; Panda, H. S.; Bahadur, D., Ice-templated Synthesis of Multifunctional Three Dimensional Graphene/Noble Metal Nanocomposites and Their Mechanical, Electrical, Catalytic, and Electromagnetic Shielding Properties. *Sci. Rep.* **2015,** *5*.
8. Wan, Y.-J.; Yu, S.-H.; Yang, W.-H.; Zhu, P.-L.; Sun, R.; Wong, C.-P.; Liao, W.-H., Tuneable Cellular-Structured 3D Graphene Aerogel and its Effect on Electromagnetic Interference Shielding Performance and Mechanical Properties of Epoxy Composites. *RSC Adv.* **2016,** *6* (61), 56589-56598.
9. Zhang, X.-J.; Wang, G.-S.; Cao, W.-Q.; Wei, Y.-Z.; Liang, J.-F.; Guo, L.; Cao, M.-S., Enhanced Microwave Absorption Property of Reduced Graphene Oxide (RGO)-MnFe2O4 Nanocomposites and Polyvinylidene Fluoride. *ACS Appl. Mater. Interfaces* **2014,** *6* (10), 7471-7478.